Icarus 394 (2023) 115437

Contents lists available at ScienceDirect

Icarus

journal homepage: www.elsevier.com/locate/icarus

Research Paper

The photochemical evolution of polycyclic aromatic hydrocarbons and nontronite clay on early Earth and Mars

Nina Kopacz [a,*], Maria Angela Corazzi [b,c], Giovanni Poggiali [b,d], Ayla von Essen [a], Vincent Kofman [e,f], Teresa Fornaro [b], Hugo van Ingen [g], Eloi Camprubi [h], Helen E. King [a], John Brucato [b], Inge Loes ten Kate [a]

[a] Department of Earth Sciences, Utrecht University, Utrecht, The Netherlands
[b] INAF Astrophysical Observatory of Arcetri, Florence, Italy
[c] Department of Physics & Astronomy, University of Florence, Florence, Italy
[d] LESIA-Observatoire de Paris, Université PSL, CNRS, Sorbonne Université, Université de Paris, Meudon, France
[e] NASA Goddard Space Flight Center, Greenbelt, MD, USA
[f] American University, Washington, DC, USA
[g] NMR Group, Bijvoet Centre for Biomolecular Research, Utrecht University, Utrecht, The Netherlands
[h] University of Texas Rio Grande Valley, Edinburg, TX, USA

ARTICLE INFO

Dataset link: https://public.yoda.uu.nl/geo/UU01/XJOBC1.html, https://doi.org/10.24416/UU01-XJOBC1

Keywords:
Early Mars
Polycyclic aromatic hydrocarbons
Clays

ABSTRACT

The photochemical evolution of polycyclic aromatic hydrocarbons (PAHs), an abundant form of meteoritic organic carbon, is of great interest to early Earth and Mars origin-of-life studies and current organic molecule detection efforts on Mars. Fe-rich clay environments were abundant on early Earth and Mars, and may have played a role in prebiotic chemistry, catalyzing the breakdown of PAHs and freeing up carbon for subsequent chemical complexification. Current Mars is abundant in clay-rich environments, which are most promising for harboring organic molecules and have comprised the main studied features by the Curiosity rover in search of them. In this work we studied the photocatalytic effects of the Fe-rich clay nontronite on adsorbed PAHs. We tested the effect of ultraviolet radiation on pyrene, fluoranthene, perylene, triphenylene, and coronene adsorbed to nontronite using the spike technique, and *in situ* diffuse reflectance infrared Fourier transform (DRIFT) spectroscopy in a Mars simulation chamber. We studied the infrared vibrational PAH bands with first order reaction kinetics and observed an extensive decrease of bands of pyrene, fluoranthene, and perylene, accompanied by the formation of PAH cations, while triphenylene and coronene remained preserved. We further analyzed our irradiated samples with nuclear magnetic resonance (NMR). Our study showed certain PAHs to be degraded via the (photo)Fenton mechanism, even under a dry, hypoxic atmosphere. Using solar spectra representative of early Earth, early Mars, and current Mars surface illumination up to 400 nm, the processes occurring in our set up are indicative of the UV-induced photochemistry taking place in Fe-rich clay environments on early Earth and Mars.

1. Introduction

Polycyclic aromatic hydrocarbons (PAHs) represent 10%–20% of cosmically available carbon (Tielens, 2013). PAHs and PAH clusters are responsible for the 3–15 μm infrared emission bands, which have been observed in remarkably similar quantities across the observable universe (Pendleton and Allamandola, 2002). Formed through combustion processes in circumstellar regions, these compounds undergo gas phase processing in the interstellar medium when subjected to ultraviolet (UV) and Lyman-α radiation and shock waves (Frenklach and Feigelson, 1989; Cherchneff et al., 1992).

Once incorporated into ice and rock in small bodies like asteroids and comets, PAHs experience a wholly different chemical evolution than in the gas phase. They can undergo hydrothermal alteration in the interiors of asteroids (Giese et al., 2019) and radiative ice processing at the surfaces of comets (Kofman et al., 2018). PAHs eventually reach planetary surfaces ferried by interplanetary dust particles (IDPs) and (micro)meteorites. Depending on their origin, the isotopic signatures of PAHs in meteorites may carry information on accretion processes and aqueous alteration conditions (Lecasble et al., 2022).

* Corresponding author.
E-mail address: k.a.kopacz@uu.nl (N. Kopacz).

https://doi.org/10.1016/j.icarus.2023.115437
Received 15 October 2022; Received in revised form 10 January 2023; Accepted 11 January 2023
Available online 18 January 2023

The further photochemical evolution of PAHs delivered to a planetary surface environment by meteoritic sources is of great interest to early Earth and Mars origin-of-life studies, as well as current organic molecule detection efforts on Mars. Both early Earth and early Mars likely experienced high luminosity in the ultraviolet part of the solar spectrum, the lack of ozone allowing the full range of UV between 200 and 400 nm to reach the surface (Cnossen et al., 2007; Claire et al., 2012; Cockell, 2000). Currently the Martian atmosphere does little to attenuate the UV flux from 200–400 nm, with an average midday flux at Gale Crater of 34.1 W m^{-2} (Vicente-Retortillo et al., 2020; Razzell Hollis et al., 2021).

Of prebiotic interest to both Earth and Mars are clay-rich environments, and the evolution of organic carbon molecules within them. On Mars, clay environments are most promising for harboring organic molecules (Grotzinger et al., 2014; Freissinet et al., 2015; Eigenbrode et al., 2018). Clay minerals on early Earth are posited to have played a role in prebiotic molecular evolution (Cairns-Smith, 1966; Hartman, 1975). Bernal first speculated on the importance of clays in this respect, because of their well-ordered arrangement, their large surface and interlayer adsorption capacity, their shielding capacity against ultraviolet radiation, their ability to concentrate organic molecules, and their ability to serve as polymerization templates (Bernal, 1949).

Abiogenesis-focused clay experiments have most often used montmorillonite, which has been shown to catalyze a large variety of organic reactions involving small molecules and PAHs (Bujdak et al., 1994; Kumar et al., 2014; Huang and Ferris, 2006; Juntunen et al., 2018), as well as serve in a protective capacity for small molecules in radiative environments (Scappini et al., 2004). However, Fe-rich smectites, and in particular nontronite, are thought to have been significantly more abundant on early Earth and Mars (Kloprogge and Hartman, 2022), and are indeed the dominant form of smectite detected on Mars (Bibring et al., 2005; Murchie et al., 2009). Little research has investigated the catalytic properties of these smectites, and it is unclear if the results obtained for montmorillonite can be directly translated to nontronite and other Fe-rich smectites (Kloprogge and Hartman, 2022). Here we explore the photochemical evolution of PAHs adsorbed to nontronite clay, and speculate on both of their roles in prebiotic carbon chemistry.

1.1. Delivery of PAHs to clay environments on early Earth

The annual flux of carbonaceous material (organic and inorganic) delivered by extraterrestrial sources to Earth is currently 300 tonnes per year (Glavin et al., 2018) and could have been as high as 10 000 to 1 million tonnes per year in the first 0.6 Ga of Earth's history (Whittet, 1997; Jenniskens et al., 2000). The significant volume of extraterrestrially delivered organic matter begs the question of whether it was a source of molecules important for prebiotic chemistry. Meteoritic organic matter is thought to be strongly associated with clay minerals in carbonaceous chondrites, wherein complex chemical evolution may already take place (Pearson et al., 2002). Much of the literature has focused on small molecules contained in meteorites, such as amino acids and nucleic acid bases, and their potential as a carbon source for prebiotic chemistry on early Earth (e.g. Marty et al. (2013)). However, 75% of extraterrestrial organic matter in meteorites is in aromatic form (Sephton, 2002), and is more likely to survive the journey to a planetary surface, during which much of the small molecules can be destroyed (Basiuk and Navarro-González, 1998; Basiuk et al., 1999). PAHs could later be broken down into smaller, more biologically relevant and reactive molecules by photolysis and photocatalysis in the ultraviolet radiation regime of early Earth (Ehrenfreund et al., 2006).

Though little is known about Earth's surface during the Hadean and early Archean, it is thought that the crust would have consisted primarily of basalt and komatiite lavas containing peridotite-derived rocks high in Fe and Mg content (O'Neil et al., 2008; Davies, 1992). The peridotite and komatiite rocks that made up the ocean floor and emerging plateaus favored the formation of Fe–Mg clay minerals upon interaction with seawater and hydrothermal alteration. The rocks would first react to trioctahedral phyllosilicates such as talc, kerolite, or stevensite-saponite, until increasing weathering would cause these to destablize and form dioctahedral Fe-rich clay minerals, with nontronite as the most abundant species (Kloprogge and Hartman, 2022).

1.2. Delivery of PAHs to clay environments on Mars

The estimated current global carbon flux on Mars from cometary impacts is 13 tonnes per year within an order of magnitude, and 50 tonnes per year from asteroids (Frantseva et al., 2018). The amount of organic material delivered to the surface of Mars by IDPs and (micro)meteorites is estimated to be of the order of 1000 tonnes per year (Flynn, 1996; Flynn et al., 2004) and would have been higher in its early history.

On Mars, ancient sedimentary environments have been found with several tens of nanomoles of carbon compounds (Grotzinger et al., 2014; Freissinet et al., 2015; Eigenbrode et al., 2018). Biological, geological, and meteoritic sources are all possible for the refractory aromatic organic material from the Sheepbed lacustrine mudstones detected by the Sample Analysis at Mars (SAM) instrument onboard the Curiosity rover (Eigenbrode et al., 2018). The diverse molecular contributions in the SAM gas chromatography-mass spectrometry (GC–MS) data from Mojave and Confidence Hills are consistent with the complex chemistry of meteoritic and geological organic matter and the interactions that occur during pyrolysis of sediments (Moldoveanu, 2009). Coevolving volatiles analyzed above 500 °C in the Mojave and Confidence Hills analyses suggest the pyrolysis of geological refractory organic macromolecules typically found in carbonaceous chondrites (Remusat et al., 2005; Okumura and Mimura, 2011).

The diversity of smectites on Mars includes nontronite, saponite, beidellite, and montmorillonite, with Fe/Mg-rich clays dominating having formed by water-restricted alteration of the original basaltic and ultramafic rocks (Kloprogge and Hartman, 2022). Another theory suggests that primordial clays on Mars were formed when Mars' primary crust reacted with a dense steam or supercritical atmosphere of water and carbon dioxide that was outgassed during magma ocean cooling (Cannon et al., 2017). Such a mechanism would have formed a widespread coherent layer of clays on the Martian surface during the pre-Noachian era.

The Martian rock record is abundant in preserved Noachian rocks. CheMin data from the Curiosity rover have shown that ancient fluviolacustrine rocks in Gale crater contain up to 35 wt.% of clay minerals (Grotzinger et al., 2014; Bristow et al., 2015). While the CheMin instrument has detected collapsed clays, i.e., with no interlayer water, these clays were likely hydrated upon their formation on early Mars, before the changing environmental conditions facilitated the desorption of structural water (Tu et al., 2021). The majority of clay minerals detected by orbital imaging spectrometers are Fe/Mg smectites in 4 billion-year-old rocks (Bibring et al., 2005; Murchie et al., 2009). Nontronite spectral signatures have been studied on the flanks of the central mount of Gale Crater (Poulet et al., 2014; Thomson et al., 2011), and have comprised the main studied features by the Curiosity rover in its search for organic molecules.

1.3. The influence of clay environments on PAHs

The widespread abundance of nontronite on early Earth and Mars would have facilitated contact with PAHs after their liberation from their meteoritic parent bodies. Nontronite has been shown to exhibit both photoprotective and photocatalytic properties to adsorbed organic molecules in the presence of UV radiation, facilitating their preservation or eventual removal (Fornaro et al., 2018b; Poch et al., 2015; dos Santos et al., 2016).

Fe-rich clays like nontronite exhibit catalytic properties: they are able to create electron–hole pairs where reaction of the holes with

adsorbed water molecules create OH radicals that can oxidize organic compounds, as first described for heterogenous catalysis on TiO_2 surfaces (Linsebigler et al., 1995; Fujishima et al., 2000). Electron–hole pairs can also induce oxidation without creating free radicals by involving chemisorbed molecules that serve as electron hole traps (Shkrob and Chemerisov, 2009; Shkrob et al., 2011a,b).

Photocatalysis has been shown to increase PAH degradation in aqueous environments under current terrestrial conditions (Wen et al., 2002; Ohno et al., 2003; Dong et al., 2010a). Environmental pollution studies have highlighted the photocatalytic effects of metal oxides and clays that facilitate the degradation of PAHs (Dong et al., 2010a,b). However, PAHs bond to mineral grains via π-cloud interactions (Campisi et al., 2021, 2022). Experiencing only weak bonds or long range interactions with their mineral substrates, the extent of photocatalytic effects on their degradation in a dry, hypoxic environment without abundant (oxi)hydroxide radical production is questioned.

In this work we experimentally tested the effect of UV radiation on different PAHs adsorbed to nontronite clay using the spike technique. Analyses were performed with *in situ* diffuse reflectance infrared Fourier transform (DRIFT) spectroscopy and nuclear magnetic resonance (NMR).

2. Materials & methods

We conducted our experiments at the INAF-Astrophysical Observatory of Arcetri, with an experimental setup in which samples were irradiated for 6 h under ambient temperature and a nitrogen atmosphere. DRIFT spectra were recorded every hour, with more frequent measurements at the beginning of each experiment. The chemical evolution of organic molecules was described with first-order reaction kinetics. We then extracted the organic fraction from the samples and analyzed them with NMR at Utrecht University.

2.1. Sample preparation

The Fe-rich clay mineral used in our experiments was selected to be representative of both early Earth and Mars and because it exhibits known catalytic properties. Natural nontronite clay was purchased from the Clay Minerals Society's Source Clays Project, where it is designated NAU-2 and is described structurally as $M^{+}_{0.72}[Si_{7.55}Al_{0.45}][Fe_{3.83}Mg_{0.05}]O_{20}(OH)_4$ (Keeling et al., 2000). Prior to the experiments the nontronite sample needed to be crushed to obtain a grain size of ~2 μm. Since manual grinding of a clay may introduce torque, preferentially straining the mineral grains in the sample, reducing tensile strength and ultimately introducing structural changes, the nontronite was ground using a Herzog HP-MA automatic pulverizing mill equipped with a tungsten-carbide vessel. This mill allows the total pressing force to be program-controlled, and ensures that no particular sheer direction is imposed on the clay lattice (Herzog, 2022).

The indigenous organics present in the clay could be removed with organic solvent washing cycles. However, this could also remove the interlayer water. Though on current Mars the clays detected are collapsed, the clays on early Earth and Mars would have likely had water in their interlayer spaces. As we do not have insight into the potential alteration of the nontronite structure due to known clay organic removal techniques (Fornaro et al., 2020) and the readmittance of water with our ensuing spike technique, we chose to use the clay in its natural state. Other studies have also chosen not to remove the indigenous organics from nontronite (dos Santos et al., 2016). We opted instead to track the chemical evolution of these organics throughout the experiment.

The PAHs used for the experiments were pyrene, perylene, fluoranthene, triphenylene, and coronene, which have all been found in meteorites (Sephton, 2002). They were purchased from Sigma Aldrich and had a purity of 98%. We adsorbed pyrene, fluoranthene, and triphenylene individually to the nontronite powder via the incipient wetness impregnation technique (Fornaro et al., 2018a), in which a molecule in solution is added to the mineral sample until it becomes a thick slurry. The volume of the solution is thus equal to the mineral porous volume. To this end we dissolved pyrene, fluoranthene, and triphenylene in toluene, which does not alter the clay mineral structure unlike other solvents such as methanol. The molecules in solution were deposited on nontronite samples to achieve a 1:100 molecule to mineral mass ratio. This ratio produced adequate infrared spectra while allowing the PAH to dry in a way that appeared evenly and thinly spread across the mineral surfaces, instead of forming large crystals as was the case when deposited in larger amounts. The samples were left to dry overnight at room temperature in a chemical hood before being measured with DRIFT spectroscopy.

Perylene and coronene do not dissolve readily in toluene, and thus they cannot be deposited via the incipient wetness technique. Instead we mechanically ground each PAH individually with the mineral powder, with the assumption that the work introduced by grinding resulted in physisorption of the two species. To obtain adequate infrared spectra (with the same intensity of organic peaks as in the samples treated with the incipient wetness technique), the molecule to mineral ratio needed to be 1:10. It should be noted that for the nontronite samples, the mechanical grinding may introduce structural changes to the mineral. However, this is not apparent in the IR data, and no clear trends between the preparation methods were found in further analyses, thus the nontronite is assumed to be identical in all samples.

For pure PAH irradiation experiments, triphenylene, perylene and coronene were introduced into the experimental apparatus directly from the bottle without any further grinding. Pyrene and fluoranthene had a larger crystal size so were first ground and then introduced into the setup. An overview of the PAHs and the experiments performed with each can be seen in Table 1.

2.2. Experimental setup

The experimental setup at INAF-Astrophysical Observatory of Arcetri allows for the *in situ* monitoring of infrared spectra of samples subjected to UV irradiation. The apparatus consists of a Bruker *Vertex 70v* FTIR double pendulum spectrometer with a Harrick *Praying Mantis*™ Diffuse Reflection Accessory for DRIFT measurements (Fig. 1). The spectrometer is interfaced with a Newport Oriel 300 W Xenon arc discharge lamp with a spectral range of 200–930 nm, which is considered a good analog source for the UV that would have reached the surface of early Earth and Mars. The total UV flux of the lamp in the spectral range of 200–400 nm is 1.94×10^{16} photons s^{-1}, as measured by a single monochromator Spectro 320 scanning spectrometer (Instrument System) (Fornaro et al., 2018a). We work in this spectral range because here the molecular absorption is higher. The radiation is focused by an optical fiber from the lamp to the spectrometer with a spot size of 800 μm onto one of two sample holders: one holder designated 'large' with radius 0.5 cm, and the other holder designated 'small' with a radius of 0.15 cm. For a spectral range of 200–400 nm, this gives a UV flux of 141 W m^{-2} for the large sample holder and 1570 W m^{-2} for the small sample holder, as compared to the average mid-day flux at Gale Crater on Mars of 34.1 W m^{-2}, calculated using the COMIMART radiative transfer model with data from the UV sensor on the Rover Environmental Monitoring Station (REMS) on board the Curiosity rover (Vicente-Retortillo et al., 2015; Razzell Hollis et al., 2021).

With this apparatus the modification of the infrared spectrum of a sample due to UV irradiation can be monitored at regular time intervals *in situ* without moving the sample itself. The reference spectrum for each PAH, recorded prior to the experiment, can be seen in Figure S1 in Appendix A. DRIFT spectroscopy measurements were taken in steps of increasing seconds for the first five minutes of irradiation, in steps of increasing minutes for the first hour, and every hour for six hours. The evolution of the PAH molecules could thus be seen in real time, with photochemical degradation manifesting itself as the decrease in peak sizes or the formation of new peaks, indicating bond breakage or new species formation, respectively.

Table 1
Overview of experiments performed. Samples were irradiated under a 300 W Xe arc lamp in a chamber at ambient temperature under a nitrogen atmosphere.

PAH	pyrene	fluoranthene	triphenylene	perylene	coronene
formula	$C_{16}H_{10}$	$C_{16}H_{10}$	$C_{18}H_{12}$	$C_{20}H_{12}$	$C_{24}H_{12}$
	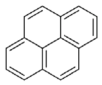	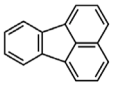	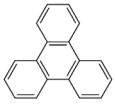	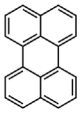	
nontronite sample preparation	incipient wetness impregnation	inc. wetness impregnation	inc. wetness impregnation	manual grinding	manual grinding
irradiation pure	6 h at 1570 Wm^{-2} (200-400 nm)				
irr. on nontronite	6 h at 141 Wm^{-2} (200-400 nm)				
analyses	FTIR, NMR	FTIR, NMR	FTIR, NMR	FTIR	FTIR

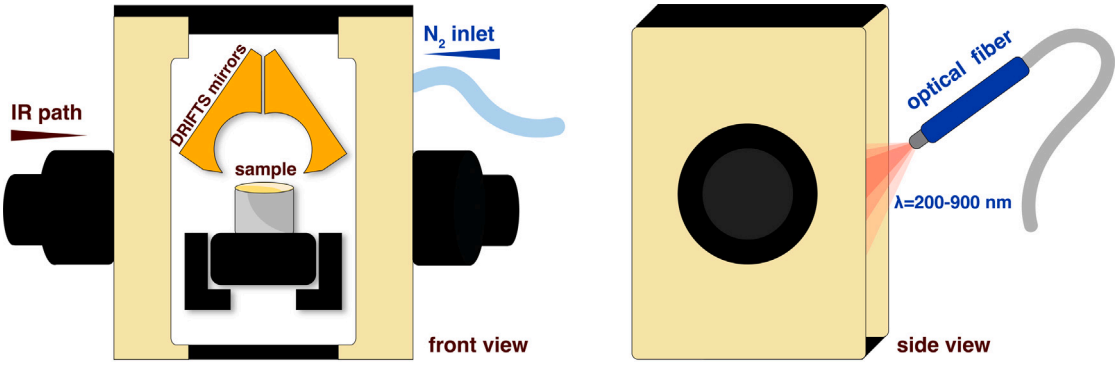

Fig. 1. Schematic of the experimental setup at INAF-Astrophysical Observatory of Arcetri. The apparatus allows for the *in situ* monitoring of infrared spectra of samples subjected to UV irradiation.

2.3. FTIR analysis

PAH infrared spectra contain a cacophony of absorption peaks due to the many vibrational modes: ring deformation, C–H out-of-plane (oop) bend, C–H in-plane (ip) bend, C–C stretch, C=C stretch, and C–H stretch. In this work the individual peaks were grouped in these categories for analysis, and the C–H in-plane bend and C–C stretch were grouped together since many of the bands overlap. Peak assignments were taken from reference spectra from the Spectral Database of Organic Compounds (SDBS) (SDBS, 2022) and the NASA Ames PAH IR Spectroscopic Database (Boersma et al., 2014; Bauschlicher et al., 2018; Mattioda et al., 2020a). The peak assignments can be seen in Table S1 in Appendix A.

The area of each peak can be seen as proportional to the amount of molecules with that vibrational mode. The peak areas were plotted against time, and the destruction or formation rates, the half-lives, and cross sections were calculated following first order kinetics relations (Cottin et al., 2003; ten Kate et al., 2005). First order kinetics assume a one-to-one interaction between one UV photon and one broken linkage in a molecule. Not all of the peaks investigated were possible to fit with one exponential function, indicating it might take more than one photon to break the corresponding bond, or multiple pathways take place. Multiphoton processes in which a PAH absorbs a second photon before it has radiated the energy of the first photon away have a low probability but can be important as well (Tielens, 2008). Such processes were not taken into account in this analysis.

The destruction rate β is calculated fitting the following first order rate equation,

$$\frac{A(t)}{A_0} = Be^{-\beta t} + C \tag{1}$$

where A_0 is the area of the peak at time $t = 0$, β is the degradation rate of the peak, B is a coefficient describing the fraction of the sample which has interacted with the radiation, and C is a coefficient describing the fraction of the sample which has not interacted with the radiation. The radiation only penetrates a few microns into the sample, whereas the IR laser penetrates much further into the sample. $B + C$ should thus equal 1.

The equation for the destruction half-life $t_{d1/2}$, or the time it takes for half of the material to be destroyed, is

$$t_{d1/2} = \frac{\ln(2)}{\beta} \tag{2}$$

where β is the degradation rate.

The cross section describes the probability of interaction between the molecule and the UV radiation. Thus the higher the cross section, the higher the chance that there will be an interaction. The destruction cross section is defined as

$$\sigma_d = \frac{\beta}{\Phi} \tag{3}$$

where β is the degradation rate and Φ is the flux of the lamp over a specified wavelength range.

Similarly, the formation rate of new species is calculated by fitting the following first order rate equation,

$$\frac{A(t)}{A_{max}} = 1 - e^{-\alpha t} \tag{4}$$

where A_{max} is the maximum peak area and α is the formation rate of the peak.

Having obtained the formation rate, we can calculate the formation half-life $t_{f1/2}$, or the time it takes for half of the reaction products to form, with $t_{f1/2} = \frac{\ln(2)}{\alpha}$. The formation cross-section is then $\sigma_f = \frac{\alpha}{\Phi}$.

Table 2
Nontronite infrared bands and assignments.
Source: Taken from Madejová (2003) and Frost et al. (2002).

Peak	Band (cm^{-1})	Vibrational mode
1	475	Si–O–Si bend
2	677	Fe–O oop bend
3	1200	Si–O stretch
4	1630	O–H bend
5	3580	O–H stretch

2.4. NMR analysis

After irradiation we recovered the samples from the setup and stored them in Eppendorf tubes for further proton NMR analysis. This was a qualitative analysis in order to see whether the irradiated samples contained any reaction products, and whether the characteristic PAH peaks showed significant changes.

We extracted the organic fraction from the nontronite samples by incubating the samples in a bath at 60 °C in a 3:1 solution of HPLC-grade methanol and chloroform. The samples were then centrifuged at 1500 rpm for 8 min. The supernatant was removed and passed through a syringe filter to eliminate any residual mineral, and subsequently dried under nitrogen overpressure.

PAH standards, pure PAH samples, and extracted samples were suspended in fully deuterated chloroform and analyzed using a 600 Bruker NMR. Deuterated chloroform was used as only non-polar breakdown products were expected from the irradiation of PAHs in a dry, hypoxic environment, where there is little water and oxygen to generate polar compounds. Standard ^{1}H 1D spectra were acquired using the zg pulse sequence, using 2.7 s acquisition time, 4 s recycle delay and 256 scans (total measurement time 30 min per 1D). Spectra were processed using exponential line broadening of 0.3 Hz before Fourier transform using Bruker Topspin and plotted in MeRestNova for the paper figures. We performed this analysis only on pyrene, fluoranthene, and triphenylene, as perylene and coronene were not sufficiently soluble in chloroform. The NMR spectra of PAHs irradiated on nontronite were compared to the PAHs irradiated pure, the PAH standards, and the experimental blanks, which consisted of the extraction solvent that had been passed through a syringe filter, then dried and resuspended in deuterated chloroform.

3. Results

3.1. Irradiation of nontronite

The infrared spectrum of pure nontronite exhibited some changes after 6 h of irradiation. The Si–O–Si, Fe–O, and Si–O infrared bands (listed in Table 2 and denoted by red numbers in Fig. 2), did not show significant changes. The O–H stretching band at 3580 cm^{-1} did narrow after irradiation as a consequence of desorption of water physisorbed on the clay, which is responsible for the broader band observed pre-irradiation in the same region and indicated by the purple line in Fig. 2. The band at 1630 cm^{-1} is attributed to the O–H bending of water in the nontronite interlayer space (Frost et al., 2002). We observe the decrease and shift of this band as some of the interlayer water is desorbed through irradiation. The bands at ~2900 cm^{-1} indicate C–H stretching in minor organic contaminants in the clay. These were not removed from the clay prior to the experiment in order to avoid possible alterations of the clay structure that might be caused by treatments usually employed to remove organics. The C–H stretching bands became more prominent post-irradiation as the absorbance of water decreased, revealing the bands of the nontronite spectrum.

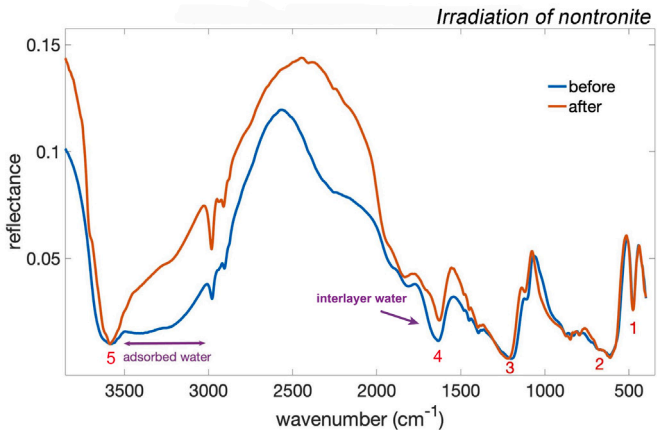

Fig. 2. DRIFT spectrum of nontronite before and after irradiation. Numbered peaks correspond to vibrational modes in Table 2.

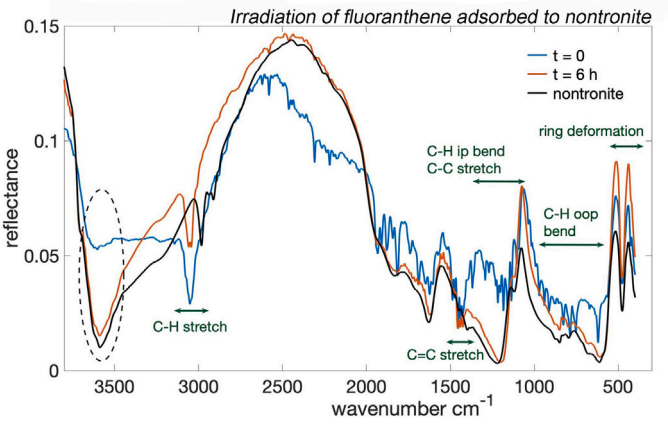

Fig. 3. FTIR reflectance spectrum of fluoranthene adsorbed to nontronite before (blue) and after (orange) irradiation, and nontronite post-irradiation (black). The dotted circle marks the OH-stretch of nontronite at 3580 cm^{-1}. (For interpretation of the references to color in this figure legend, the reader is referred to the web version of this article.)

3.2. Irradiation of PAHs

We monitored the irradiation of PAHs *in situ* with DRIFT spectroscopy, with measurements taken in steps of increasing seconds for the first five minutes of irradiation, in steps of increasing minutes for the first hour, and every hour for six hours. All PAHs were irradiated pure and adsorbed to nontronite (Table 1).

Fig. 3 shows the FTIR spectrum of fluoranthene adsorbed to nontronite before irradiation (in blue) and after 6 h of irradiation (in orange), where all of its characteristic peaks have decreased or disappeared entirely, revealing the underlying spectrum of nontronite. The nontronite band at 3580 cm^{-1} (O–H stretch, marked with a dotted circle in Fig. 3), which was obscured by the more prominent fluoranthene spectrum prior to irradiation, is visible post-irradiation. We modeled the decay of peaks with Eqs. (1)–(4). The decay parameters of fluoranthene bands are listed in Table 3. The C–H in-plane bend and C–C stretch were grouped in one category, since many of the bands overlap. The parameters for the different bands are in a similar range and were averaged to give parameters for the total molecule.

We observed the degradation of perylene when adsorbed to nontronite and exposed to UV for 6 h (Fig. 4a), as well as the growth of some peaks (Fig. 4b). The perylene bands that decreased did so at similar rates, though many of the perylene bands could not be modeled with Eqs. (1)–(4) (Table S1, Figure S6 in Appendix A), and were thus

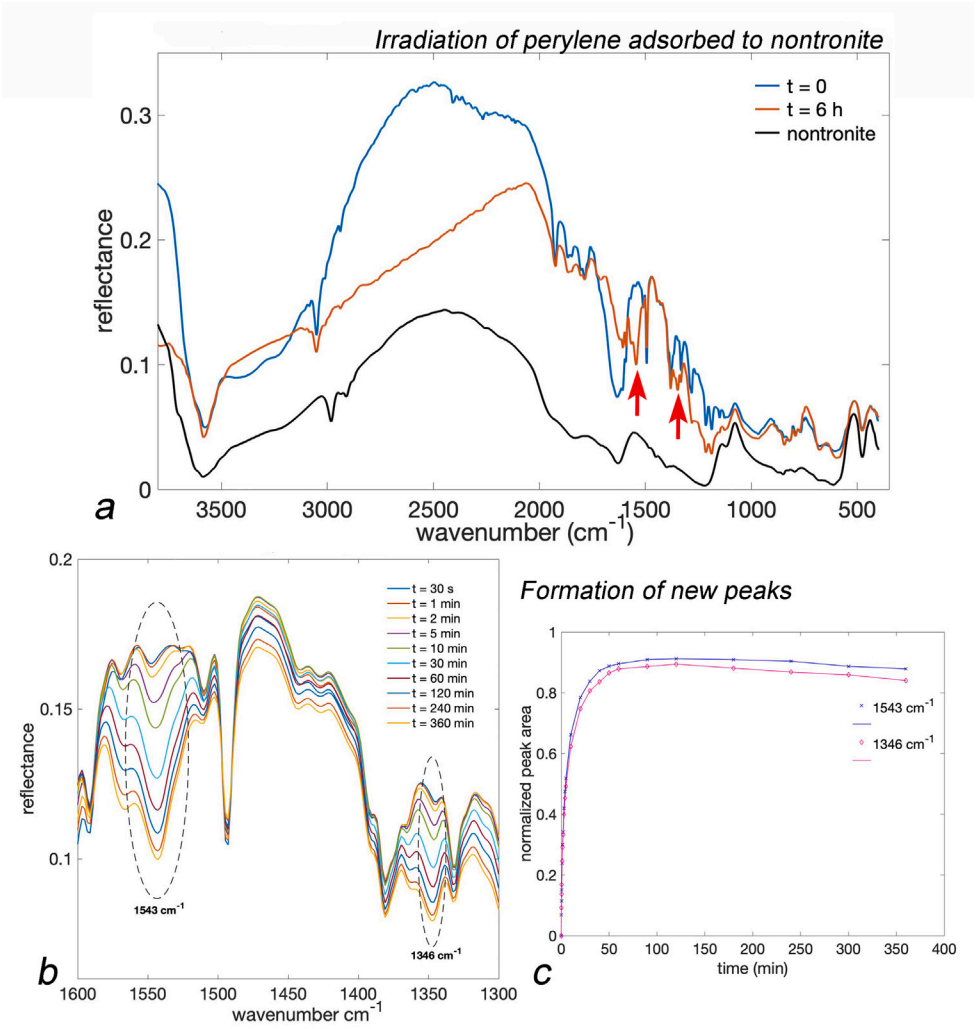

Fig. 4. FTIR spectra of perylene adsorbed to nontronite before and after irradiation, compared to the spectrum of nontronite post-irradiation (a), (b) formation of new peaks during irradiation of perylene (indicated by red arrows in (a)), (c) reaction kinetics of new peaks shown in (b).

Table 3
Degradation kinetics of UV-irradiated fluoranthene ($C_{16}H_{10}$) adsorbed to nontronite. Parameters were calculated with Eqs. (1)–(4).

Mode	$t_{d1/2}$ (min)	σ_d ($\times E^{-19} cm^2$)
Ring deformation	83 ± 21	3 ± 1
C–H oop bend	69 ± 32	10 ± 4
C–H ip bend/ C–C stretch	62 ± 13	5 ± 1
C=C stretch	74 ± 17	4 ± 1
Total molecule	**72 ± 20**	**6 ± 2**

oop: *out-of-plane*, *ip*: *in-plane*.

not included in the analysis. The formation of two bands in the C=C range is pointed out with red arrows in Fig. 4a, and manifests as the growth and rightward shift of bands at 1543 cm^{-1} and 1346 cm^{-1} (Fig. 4b). The formation kinetics of new bands is shown in Fig. 4c, and is consistent with the formation of perylene cations (Szczepanski et al., 1993). However, there should also be a rightward shift and growth of the peak at 1334 cm^{-1} to 1318 cm^{-1}, which we do not observe. This could be due to the stifling of certain vibrations because of mineral matrix or PAH crystal effects, which do not allow the PAHs to vibrate freely as they would in the gas phase. This could also explain the differences in the intensities of the 1543 cm^{-1} and 1346 cm^{-1} bands between our experiments and those reported in the literature for gas phase or matrix-isolated species. In addition, the area around 1318 cm^{-1} is very crowded with intense underlying nontronite bands. This could obscure detection of the 1318 cm^{-1}, if it is present.

The formation of PAH ion peaks generally show an initial growth before plateauing off or slightly decreasing due to photobleaching of the ions (Mattioda et al., 2020a; Hudgins and Allamandola, 1997; Hudgins and Sandford, 1998), as seen in our results in Fig. 4c. Photoproducts, on the other hand, would increase linearly with time (Mattioda et al., 2020a), and any PAH hydrogenation would be associated with the growth of C–H stretching bands in the 2800–3000 cm^{-1} region (Cruz-Diaz et al., 2020), which we do not observe as the perylene C–H band in that region is degraded (Table 5). However, the growth of the 1543 cm^{-1} and 1346 cm^{-1} bands could alternatively be indicative of C–H bending bands (Mattioda et al., 2020b), suggesting the hydrogenation of the perylene molecules. Whether we are observing the formation of perylene cations or rather the hydrogenation of perylene molecules could be hinted at by which of the two are more stable on the nontronite surface. Previous work has shown that PAH radical cations can persist on irradiated clay surfaces for several hours in an oxic environment, before they are further broken down by reactive oxygen species (Jia et al., 2019). As the atmosphere in our experiments is largely anoxic, we could expect both perylene cations and hydrogenated perylene to remain stable for the length of the experiment.

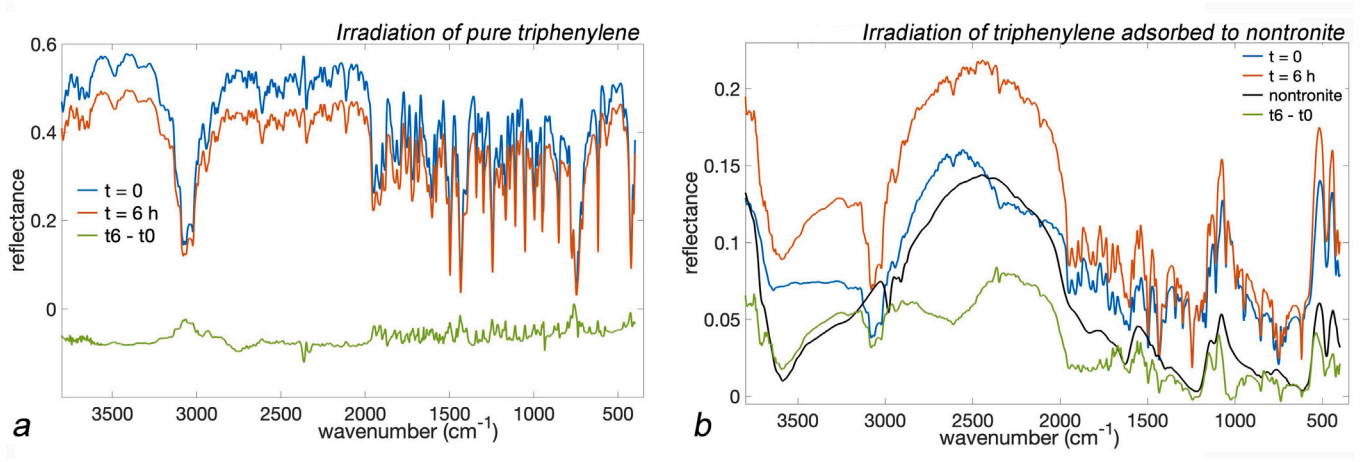

Fig. 5. FTIR spectra of triphenylene ($C_{18}H_{12}$) irradiated pure (a) and adsorbed to nontronite (b). The nontronite spectrum post-irradiation is shown in black, and the difference spectra of triphenylene (spectrum at t = 0 subtracted from spectrum at t = 6) are shown in green. (For interpretation of the references to color in this figure legend, the reader is referred to the web version of this article.)

Table 4
Reaction kinetics of UV-irradiated triphenylene pure and adsorbed to nontronite. Parameters were calculated with Eqs. (1)–(4).

Triphenylene	Pure		On nontronite	
Mode	$t_{d1/2}$ (min)	$\sigma_d \times E^{-19}$ (cm^2)	$t_{f1/2}$ (min)	$\sigma_f \times E^{-19}$ (cm^2)
Ring deformation	200 ± 120	0.15 ± 0.08	13 ± 4	22 ± 9
C–H oop bend	230 ± 130	0.14 ± 0.06	17 ± 7	17 ± 8
C–H ip bend/C–C stretch	97 ± 37	0.28 ± 0.09	8 ± 2	62 ± 32
C=C stretch	110 ± 33	0.34 ± 0.01	7 ± 3	40 ± 20
C–H stretch	94 ± 29	0.3 ± 0.1	10 ± 4	29 ± 14
Total molecule	**150 ± 69**	**0.23 ± 0.09**	**11 ± 4**	**34 ± 17**
Flux (Wm^{-2})	1570		141	

oop: out-of-plane, ip: in-plane, $t_{d1/2}$: destruction half-life, σ_d: destruction cross section, $t_{f1/2}$: formation half-life, σ_f: formation cross section.

When pure PAHs were irradiated, only the spectrum of triphenylene exhibited changes (Fig. 5a), while no changes were observed in the spectra of pyrene, perylene, fluoranthene, and coronene (Figure S2 in Appendix A). While pure triphenylene manifested peak degradation during irradiation, triphenylene on nontronite exhibited peak growth (Fig. 5b) at similar rates for all peaks. This indicates preservation of the molecule: the slight growth of peaks at the beginning of the experiment is probably due to the rearranging of the PAH molecules in the sample due to minimal heating effects. The peak degradation and growth kinetics of triphenylene are compared in Table 4.

The reaction kinetics of all PAHs adsorbed to nontronite are listed in Table 5. Pyrene, fluoranthene, and perylene were degraded in the presence of UV and nontronite, with at least half of the PAHs removed after 6 h of irradiation. Triphenylene and coronene exhibited peak growth in the presence of UV and nontronite, indicating the retention of the PAHs in the samples during 6 h of irradiation. Again, the growth of the IR bands is rather due to the rearranging of the PAH molecules in the sample at the start of the experiment rather than the formation of new products, as there are no new peaks forming. Desorption of PAH molecules by the UV lamp or the IR beam was discounted, based on temperature measurements of the sample area and previous work in the setup, which has not encountered issues with such effects (Potenti et al., 2018; Poggiali et al., 2020; Fornaro et al., 2018a). The spectra pre- and post-irradiation of all UV-irradiated PAHs adsorbed to nontronite are shown in Figure S3 and their reaction kinetics in Figures S4–S6 in Appendix A.

The clay-related organic contaminants at ~3000 cm^{-1} (Fig. 2), which were not removed from the clay, were also subject to the irradiation experiments. The degradation of the band at ~3000 cm^{-1} belonging to the contaminants may contribute slightly to the parameters calculated for the C–H stretch of perylene, triphenylene, and coronene. However, the overall behavior of the bands is reflecting changes in the PAH molecules, given that their kinetics are in line with the kinetics of the other bands (Table 5). For pyrene and fluoranthene the kinetics of the band at ~3000 cm^{-1} were discounted, as they exhibited behavior much different to that of the other bands. This may indicate that the behavior of that band was dominated by the eventual degradation of the organic clay-related contaminants.

3.3. Extractions of PAHs post-irradiation

Pyrene, fluoranthene, and triphenylene samples recovered from the irradiation experiments were further analyzed with NMR (Fig. 6). The NMR spectra of PAHs irradiated on nontronite were compared to the PAHs irradiated pure, the PAH standards, and the experimental blanks. Note that the NMR studies are purely qualitative.

The spectra of pure, irradiated, and clay-irradiated PAHs were superimposed (Fig. 6a, c, e) and scaled to match the intensities of the characteristic PAH aromatic peaks. This allowed us to detect changes in relative peak intensities indicating degradation. In the pyrene and fluoranthene clay-irradiated samples (Fig. 6a, c), the characteristic PAH peaks decreased strongly in intensity relative to the small aromatic peaks in the region, indicating the degradation of the PAHs. These smaller signals surrounding the PAH peaks are likely from aromatic impurities as they are also present in the pure PAH samples but at much lower intensity to the pure PAH signals. Based on the change in relative intensity, about 30% of pyrene and 40% of fluoranthene were degraded.

Further analysis of the spectra showed that a new shoulder formed on the clay-irradiated pyrene peak at 8.18 ppm, indicating the presence of a possible partly degraded PAH intermediate (pointed out with a black arrow in Fig. 6a). A few more new peaks appeared in the clay-irradiated samples at ~3.5 ppm (the range of alcohols) in the pyrene and triphenylene samples (indicated by black arrows in Fig. 6b, f).

Table 5
Reaction kinetics of UV-irradiated PAHs adsorbed to nontronite. Parameters were calculated with Eqs. (1)–(4). The destruction half-life ($t_{d1/2}$), destruction cross section (σ_d), formation half-life ($t_{f1/2}$) and formation cross section (σ_f) are given for each vibrational mode for the corresponding PAH, and averaged for the total molecule. The C–H in-plane bend and C–C stretch are grouped in one category, since many of the bands overlap.

	PAH	Pyrene	Fluoranthene	Perylene	PAH	Triphenylene	Coronene
Mode	**Degradation**	$C_{16}H_{10}$	$C_{16}H_{10}$	$C_{20}H_{12}$	**Retention**	$C_{18}H_{12}$	$C_{24}H_{12}$
Ring deformation	$t_{d1/2}$ (min) $\sigma_d \times E^{-19}$ (cm^2)	220 ± 65 1.4 ± 0.7	83 ± 21 3 ± 1	n/a n/a	$t_{f1/2}$ (min) $\sigma_f \times E^{-19}$ (cm^2)	13 ± 4 22 ± 9	4 ± 3 81 ± 87
C–H oop bend	$t_{d1/2}$ (min) $\sigma_d \times E^{-19}$ (cm^2)	80 ± 9 3.8 ± 0.8	69 ± 31 10 ± 4	77 ± 33 4 ± 2	$t_{f1/2}$ (min) $\sigma_f \times E^{-19}$ (cm^2)	17 ± 7 17 ± 8	n/a n/a
C–H ip bend C–C stretch	$t_{d1/2}$ (min) $\sigma_d \times E^{-19}$ (cm^2)	180 ± 42 1.6 ± 0.5	62 ± 13 5 ± 1	49 ± 10 6 ± 2	$t_{f1/2}$ (min) $\sigma_f \times E^{-19}$ (cm^2)	8 ± 2 62 ± 32	n/a n/a
C=C stretch	$t_{d1/2}$ (min) $\sigma_d \times E^{-19}$ (cm^2)	210 ± 55 1.4 ± 0.5	74 ± 17 4 ± 1	n/a n/a	$t_{f1/2}$ (min) $\sigma_f \times E^{-19}$ (cm^2)	7 ± 3 40 ± 20	2.5 ± 0.6 120 ± 43
C–H stretch	$t_{d1/2}$ (min) $\sigma_d \times E^{-19}$ (cm^2)	n/a n/a	n/a n/a	40 ± 10 7 ± 2	$t_{f1/2}$ (min) $\sigma_f \times E^{-19}$ (cm^2)	10 ± 4 29 ± 14	7 ± 3 39 ± 22
Total molecule	$t_{d1/2}$ (min) $\sigma_d \times E^{-19}$ (cm^2)	170 ± 43 2.0 ± 0.6	72 ± 20 6 ± 2	55 ± 17 6 ± 2	$t_{f1/2}$ (min) $\sigma_f \times E^{-19}$ (cm^2)	11 ± 4 34 ± 17	4 ± 2 79 ± 51

oop: out-of-plane, ip: in-plane
$t_{d1/2}$: destruction half-life, σ_d: destruction cross section
$t_{f1/2}$: formation half-life, σ_f: formation cross section.

Fluoranthene already has this shift in its standard spectra, and a shift here could also be attributed to indigenous organics within the clay structure. The other new signals in the clay-irradiated samples are accounted for by the experimental blanks.

4. Discussion

4.1. Effect of UV on nontronite

Fe-rich clays like nontronite can exhibit catalytic properties in the presence of UV radiation: they can create electron–hole pairs that can react either with adsorbed water molecules creating hydroxyl radicals, or with chemisorbed molecules that serve as electron hole traps (Linsebigler et al., 1995; Fujishima et al., 2000; Shkrob et al., 2011a,b). The presence of water physisorbed on the clay and the structural water of the clay could result in the production of OH radicals that may facilitate the Fenton mechanism (Fenton, 1894). The Fenton reaction results in the oxidation of Fe^{2+} to Fe^{3+},

$$Fe^{2+} + H_2O_2 \rightarrow Fe^{3+} + OH^{\bullet} + OH^{-} \quad (5)$$

The photo-Fenton reaction is enhanced by UV light at wavelengths <350 nm, producing additional OH radicals, and leading to Fe^{3+} reduction (Ruppert et al., 1993),

$$Fe^{3+} + OH^{-} \xrightarrow{h\nu(<350\ nm)} Fe^{2+} + OH^{\bullet} \quad (6)$$

and regeneration of the catalyst,

$$HO^{\bullet} + OH^{\bullet} \rightarrow H_2O_2 \quad (7)$$

In our experiments, Reactions (6) and (7) described above can generate Fe^{2+} and OH, producing H_2O_2, and facilitating the Fenton mechanism leading to the reduction of the clay,

$$Fe(III)smectite + OH^{-} \xrightarrow{h\nu(<350\ nm)} Fe(II)smectite + OH^{\bullet} \quad (8)$$

The clay may be subject to subsequent reoxidation by H_2O_2 (Jia et al., 2012; Yap et al., 2011),

$$Fe(II)smectite + H_2O_2 \rightarrow Fe(III)smectite + OH^{\bullet} + OH^{-} \quad (9)$$

or in the presence of oxygen,

$$Fe(II)smectite + O_2 \rightarrow Fe(III)smectite + O_2^{-} \quad (10)$$

forming superoxide radicals (Sỳkora, 1997).

The OH radicals and H_2O_2 can further catalyze the photo-Fenton reaction and can oxidize PAHs adsorbed to the mineral surface. The hypoxic experimental conditions in our experiments likely inhibit Reaction (10), in part stifling subsequent oxidation of reduced nontronite. Nonetheless, the Fenton mechanism can proceed following the ionization of surface and interlayer water molecules and OH groups by UV radiation. This is supported by the decrease in the O–H bending and stretching bands in the nontronite IR spectrum post irradiation (Fig. 2). The removal of interlayer water from the clay is indicative of the processes occurring on Mars, where the CheMin instrument has detected collapsed clays, i.e., with no interlayer water (Tu et al., 2021). The interlayer water was likely removed from these clays over time, facilitated by the changing environmental conditions, particularly the increasingly harsh radiative environment.

The catalytic activity of nontronite is excellent over a wide pH range, with nontronite remaining both chemically and mechanically stable, with no measurable Fe leaching, damage to the structure, or noticeable loss of activity (Liu et al., 2014). Reduction in nontronite occurs to the greatest extent in the octahedral sheet iron and oxidation in the tetrahedral sheet iron (Geatches et al., 2012). Reduction of octahedral iron causes a change in specific surface area of the smectite sheets, Lear and Stucki (1989) which can reduce the interlayer spacing and trap interlayer cations, ultimately changing the reactivity of the clay. Fe^{2+} and Fe^{3+} act as photocatalysts via the Fenton mechanism at low pHs (≤4) (Fenton, 1894). Nontronite has the potential to have high surface acidity, due to exchangeable cations in its interlayer space (Laszlo, 1987). This will be more important in a dry environment, with no water molecules to react with to reduce the acidity. Carbocations formed here can further react with interlayer water to produce alcohols and ethers (Theng, 2018; Adams et al., 1979; Nagendrappa et al., 2002). This may explain the appearance of additional peaks at ~3.5 ppm in our NMR spectra of the organic extractions of clay-irradiated samples (Fig. 6).

Conversely, Fe-rich minerals can be strong absorbers of UV light, which can provide protection against radiation damage (Pierson et al., 1993; Gauger et al., 2015). Nontronite has been shown to exhibit a photoprotective effect on adsorbed amino acids when irradiated with UV under current Martian surface conditions (Poch et al., 2015; dos Santos et al., 2016). These results suggest that photoprotection by nontronite is not only due to mechanical shielding (elevated because of the clay's high surface area and small pore sizes) (dos Santos et al., 2016), but also caused by stabilizing interactions between the molecules and the mineral surface, which allow absorbed energy to dissipate and photodissociated molecules to recombine (Poch et al., 2015).

Nontronite's high surface area also creates more sites for PAH adsorption to the clay and potential for PAHs to experience the catalytic

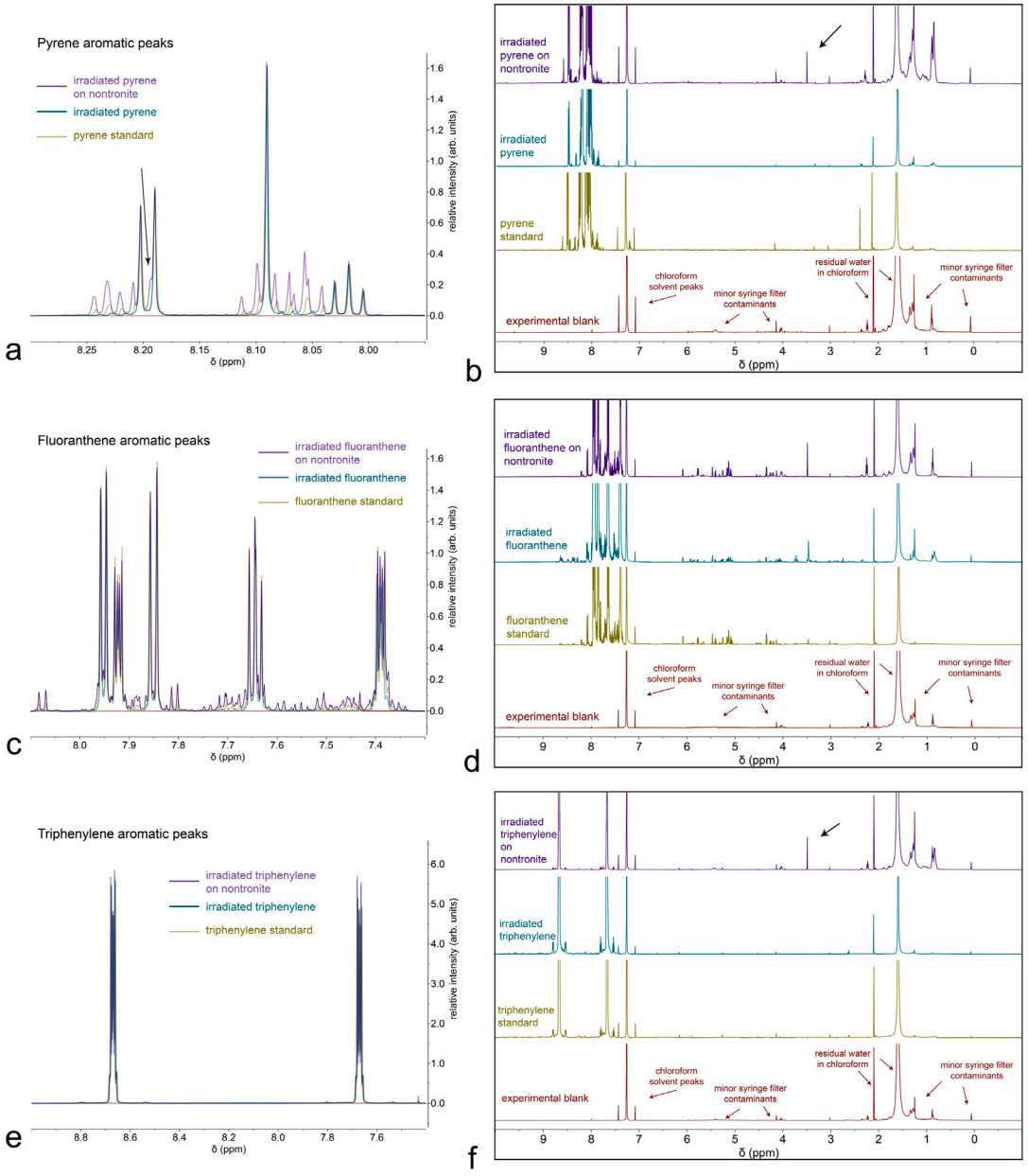

Fig. 6. NMR data of irradiated samples. Pure PAHs and PAHs extracted from clay samples are compared to PAH standards and experimental blanks. (a–b) spectra of pyrene, (c–d) spectra of fluoranthene, (e–f) spectra of triphenylene. The data are normalized to the intensity of the PAH peaks. New peaks or shoulders are marked with black arrows. The superimposed spectra were scaled to match the intensities of the characteristic PAH aromatic peaks, revealing potential changes in relative peak intensities. (For interpretation of the references to color in this figure legend, the reader is referred to the web version of this article.)

effects of Fe in the clay. Thus nontronite can exhibit both photoprotective and photocatalytic effects, with the dominant effect seeming to vary per PAH, as described in the next section.

4.2. Effect of UV on PAHs

The adsorption of PAHs to Fe-rich clay minerals is likely accompanied by the formation of "cation-π" interactions at the active sites, inducing electron transfer from PAHs to surface cations (Jia et al., 2018). This would result in oxidation of the PAH,

$$\text{Fe(III)smectite} - \text{PAH} \xrightarrow{h\nu(<350\ \text{nm})} \text{Fe(II)smectite} - \text{PAH}^{+} \quad (11)$$

and further oxidation of the PAH by radicals and H_2O_2 produced in Reactions (7)–(10).

In previous work, the photodegradation of pyrene in solid state on various Fe oxide surfaces had a half-life of 3 to 4 h depending on the Fe oxide, calculated by extracting and measuring pyrene concentration over irradiation time (Wang et al., 2009). Pyreno was identified as an intermediary reaction product by gas chromatography-mass spectrometry (GC–MS). Similarly, the photodegradation of pyrene on TiO_2 and soil surfaces was studied, and all loss of pyrene was attributed to ionization by the Fenton mechanism (Zhang et al., 2008, 2010).

The photodegradation of phenanthrene under visible light (380–780 nm) was found to follow a pseudo-first-order kinetic model when adsorbed to smectite saturated with Fe^{3+} cations, with 100% loss after 6 h of irradiation (Jia et al., 2012). They attributed the degradation to the photo-Fenton effect, wherein hydroxyl radicals and singlet oxygen preferentially attack phenanthrene at positions 9 and 10, eventually leading to the production of 9,10-Phenanthrenequinone, phthalate,

Table 6
Comparing the effect of nontronite on adsorbed irradiated PAHs. Parameters were calculated with Eqs. (1)–(4). The halflives were extrapolated to reflect current surface conditions on Mars, where the average mid-day flux at Gale Crater was calculated using the COMIMART radiative transfer model (Vicente-Retortillo et al., 2015; Razzell Hollis et al., 2021).

PAH	pyrene	fluoranthene	perylene	**PAH**	triphenylene	coronene
degradation	$C_{16}H_{10}$ 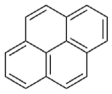	$C_{16}H_{10}$ 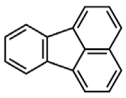	$C_{20}H_{12}$ 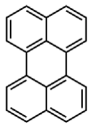	**retention**	$C_{18}H_{12}$ 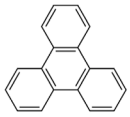	$C_{24}H_{12}$ 
in the lab where $\Phi = 141$ Wm^{-2} (200-400 nm)						
$t_{d1/2}$ (min)	170±43	72±20	55±17	$t_{f1/2}$ (min)	11±4	4±2
$\sigma_d \times E^{-19}$(cm^2)	2.0±0.6	6±2	6±2	$\sigma_f \times E^{-19}$(cm^2)	34±17	79±51
on Mars where $\Phi = 34.1$ Wm^{-2} (200-400 nm)						
$t_{d1/2}$ (sol)	0.5±0.1	0.20±0.06	0.15±0.05	$t_{f1/2}$(sol)	0.03±0.01	0.012±0.007
effect of nontronite	catalytic	catalytic	catalytic		protective	protective

diisobutyl phthalate and various alkanes, such as esters, alkanoic acids, alkanols, alkanes, and dioxanes.

Similarly in our experiments, Reaction (8) described above is thought to have generated Fe^{2+}, producing H_2O_2 and facilitating the Fenton mechanism (Jia et al., 2012; Yap et al., 2011), which would have degraded the adsorbed PAHs, along with direct oxidation by OH radicals and water molecules removed from the clay by UV, and the electron transfer in Reaction (11). Interestingly, only pyrene, fluoranthene, and perylene show degradation in their IR spectra and seem to be significantly affected by this mechanism. Though probably experiencing only weak bonding or long range interactions with the nontronite surface (Campisi et al., 2021, 2022), in our experiments pyrene, fluoranthene, and perylene were subject to photodegradation under a dry, hypoxic atmosphere. A summary of the results can be seen in Table 6. The averaged total molecule half-lives and cross sections were compared, and scaled with the average mid-day flux at Gale Crater on Mars of 34.1 W m^{-2} (in the 200–400 nm range) (Vicente-Retortillo et al., 2015; Razzell Hollis et al., 2021), to reflect their significance on the surface of present Mars.

Because of their aromaticity, PAHs are inherently stable molecules with large electronic absorption cross-sections, which makes them strong absorbers of UV light. They are also stable as ions, and are thought to be present both positively and negatively charged in the interstellar medium; when PAHs are ionized the strength of modes in their IR spectra involving C–C stretching vibrations can increase manifold, whereas the C–H stretching and, to a lesser extent, the out-of-plane bending vibrations decrease in strength (Tielens, 2008). In our experiments, the spectra of perylene showed evidence of PAH ions, with the formation of new peaks in the C=C range (Fig. 4b, c) and a decrease in the C–H band. However, we were not able to determine whether perylene was forming cations or rather undergoing hydrogenation, owing to the difficulty in comparing infrared spectra from our samples with spectra of perylene in the gas phase. The gaps between our understanding of PAH photochemistry in the gas phase, in ice matrices, and in mineral matrices warrant a full-scale analytical campaign.

The trends we see in our experiments hold up across the different sample preparation techniques we have used. Our NMR data supports the FTIR data, showing that clay-irradiated pyrene and fluoranthene degraded. The lack of major reaction products in the NMR data could be due to any breakdown products degrading immediately into small volatile hydrocarbons and carbon dioxide (which would not be present in high enough concentrations to cause a change in the spectrum in a DRIFTS type set up). The extraction technique used targeted solid-state products as these are expected to be non-polar given the nature of the parent molecule and the dry, hypoxic experimental conditions. Instead the PAHs may well be degrading directly into CO, CO_2, C_2H_2, CH_3OH and other small hydrocarbons, which are volatile and readily escape from the system. This is supported by laboratory results of irradiated PAHs adsorbed to forsterite and anatase, where solid state photodegradation of the PAHs resulted in the production of CO_2 (Potenti et al., 2018).

Triphenylene and coronene were not degraded by photocatalysis on the surface of nontronite, possibly owing to different binding geometries and adsorption mechanisms between the PAH and the clay surface. If the PAHs are not strongly bound to the surface, they may not be affected by the electron transfer reaction and oxidizing radicals produced by the Fenton mechanism (Reactions (8)–(11)). In general the binding energy increases with the PAH size/surface area, a trend attributed to the increasing number of contact points (though pyrene is an exception to this, having higher binding energies than fluoranthene because of its more compact geometry) (Campisi et al., 2022). Conversely triphenylene in our experiments may have a lower binding energy because of its less compact geometry, facilitating its preservation. Adsorption energies depend also on the specific geometrical interaction of the PAH and the mineral surface, and might not have such a straightforward trend, especially with a complex mineral like nontronite.

Triphenylene was shown to degrade when irradiated pure, but was completely preserved when irradiated with nontronite, indicating the clay may be serving in a protective capacity by shielding the PAH from UV radiation. While coronene is stable in pure form, it can be that part of the UV radiation was absorbed by nontronite when they were irradiated together, but its inefficient adsorption to the grains made it immune to the clay's catalytic effects. Alternatively, it is possible a large PAH like coronene with a large electronic absorption cross section absorbed more of the UV radiation, shielding the nontronite and preventing it from forming the required precursors for the Fenton reactions. It is likely the inefficient adsorption of triphenylene and coronene to nontronite grains and/or the large UV absorption capability of coronene are facilitating their deliverance from the photocatalytic effects of nontronite clay.

5. Conclusion

Our UV irradiation experiments of various polycyclic aromatic hydrocarbons (PAHs) adsorbed to nontronite showed both degradation and retention of PAH molecules (Table 6). The degradation of pyrene and fluoranthene was manifested by the decrease of infrared bands and characteristic NMR aromatic peaks. The formation of new peaks in the perylene spectra indicated the formation of perylene cations or

hydrogenation of perylene molecules. The triphenylene and coronene IR bands showed no decrease throughout irradiation, indicating the preservation of the molecules. The degradation of PAHs was attributed to the Fenton mechanism resulting from the photocatalytic activity of the irradiated Fe-rich smectite nontronite. Our results indicate the removal of adsorbed and interlayer water from irradiated nontronite, which facilitates the Fenton mechanism and is indicative of processes on Mars, where the observed clays are collapsed, i.e., with no interlayer water. The interlayer water was likely removed from these clays over time, facilitated by the changing environmental conditions, particularly the increasingly harsh radiative environment.

The effect of the Fenton mechanism on PAHs likely depends on their adsorption capacity on nontronite, and their electronic absorption cross section. While nontronite may exhibit both catalytic and protective properties when irradiated with UV, it may also be that PAHs with large electronic cross section can in turn shield nontronite, preventing it from forming the required precursors for the Fenton mechanism. The efficiency of this mechanism thus varies depending on the combination of all these factors, with no straightforward trend. While certain PAHs may have broken down and contributed organic carbon to prebiotic chemistry on clays, others may have remained inert. There exist difficulties in studying PAHs in prebiotic environments, owing to discrepancies in the behavior of infrared spectra between PAHs in experiments like ours and PAHs in the gas phase. The gaps between our understanding of PAH photochemistry in the gas phase, in ice matrices, and in mineral matrices warrant a full-scale analytical campaign.

Assuming the simulated solar spectra used in this study are representative of early Earth, early Mars, and current Mars surface illumination up to 400 nm, the processes occurring in our set up are indicative of the UV-induced photochemistry taking place in Fe-rich clay environments on early Earth and Mars. We have demonstrated that degradation of PAHs on nontronite via the Fenton mechanism is possible, even under a dry, hypoxic atmosphere. Thus certain meteoritic PAHs were likely degraded into smaller organic molecules on the Martian surface, which should be considered when determining the sources of organic molecules detected by Mars rovers. Future organic molecule irradiation experiments in Martian conditions could explore the reactivity of different kinds of smectites, such as Mg-smectites, and sulfates.

Data availability

The data supplement to this work is freely accessible at https://public.yoda.uu.nl/geo/UU01/XJOBC1.html, https://doi.org/10.24416/UU01-XJOBC1.

Acknowledgments

This work was supported by the Dutch Research Council (NWO), The Netherlands grant ALWOP.274. E.C. is grateful to NWO, The Netherlands for an Origins Center Fellowship. The work of M.A.C., G.P., T.F., and J.B. was supported by the Italian Space Agency (ASI) grant agreement ASI/INAF n. 2017-48-H-0. The work of H.v.I. was supported by NWO ENW Roadmap, The Netherlands grant 00901157 to the uNMRnl consortium. Thanks to two anonymous reviewers for insightful comments and to Andrew Mattioda for fruitful discussions.

Appendix A. Supplementary data

Supplementary material related to this article can be found online at https://doi.org/10.1016/j.icarus.2023.115437.

References

Adams, J.M., Ballantine, J.A., Graham, S.H., Laub, R.J., Purnell, J.H., Reid, P.I., Shaman, W.Y., Thomas, J.M., 1979. Selective chemical conversions using sheet silicate intercalates: Low-temperature addition of water to 1-alkenes. J. Catal. 58 (2), 238–252.

Basiuk, V., Douda, J., Navarro-Gonzalez, R., 1999. Transport of extraterrestrial biomolecules to the Earth: problem of thermal stability. Adv. Space Res. 24 (4), 505–514.

Basiuk, V.A., Navarro-González, R., 1998. Pyrolytic behavior of amino acids and nucleic acid bases: Implications for their survival during extraterrestrial delivery. Icarus 134 (2), 269–278.

Bauschlicher, C.W., Ricca, A., Boersma, C., Allamandola, L., 2018. The NASA Ames PAH IR spectroscopic database: Computational version 3.00 with updated content and the introduction of multiple scaling factors. Astrophys. J. Suppl. Ser. 234 (2), 32.

Bernal, J.D., 1949. The physical basis of life. Proc. Phys. Soc. A 62 (9), 537.

Bibring, J.-P., Langevin, Y., Gendrin, A., Gondet, B., Poulet, F., Berthé, M., Soufflot, A., Arvidson, R., Mangold, N., Mustard, J., et al., 2005. Mars surface diversity as revealed by the OMEGA/Mars Express observations. Science 307 (5715), 1576–1581.

Boersma, C., Bauschlicher, C., Ricca, A., Mattioda, A., Cami, J., Peeters, E., de Armas, F.S., Saborido, G.P., Hudgins, D., Allamandola, L., 2014. The NASA ames PAH IR spectroscopic database version 2.00: Updated content, web site, and on (off) line tools. Astrophys. J. Suppl. Ser. 211 (1), 8.

Bristow, T.F., Bish, D.L., Vaniman, D.T., Morris, R.V., Blake, D.F., Grotzinger, J.P., Rampe, E.B., Crisp, J.A., Achilles, C.N., Ming, D.W., et al., 2015. The origin and implications of clay minerals from Yellowknife Bay, Gale crater, Mars. Am. Mineral. 100 (4), 824–836.

Bujdak, J., Slosiarikova, H., Texler, N., Schwendinger, M., Rode, B., 1994. On the possible role of montmorillonites in prebiotic peptide formation. Monatsh. Chem./Chem. Mon. 125 (10), 1033–1039.

Cairns-Smith, A.G., 1966. The origin of life and the nature of the primitive gene. J. Theoret. Biol. 10 (1), 53–88.

Campisi, D., Lamberts, T., Dzade, N.Y., Martinazzo, R., ten Kate, I.L., Tielens, A.G., 2022. Adsorption of polycyclic aromatic hydrocarbons and C60 onto forsterite: C–H bond activation by the schottky vacancy. ACS Earth Space Chem..

Campisi, D., Lamberts, T., Dzade, N.Y., Martinazzo, R., Ten Kate, I.L., Tielens, A.G., 2021. Interaction of aromatic molecules with forsterite: accuracy of the periodic DFT-D4 method. J. Phys. Chem. A 125 (13), 2770–2781.

Cannon, K.M., Parman, S.W., Mustard, J.F., 2017. Primordial clays on Mars formed beneath a steam or supercritical atmosphere. Nature 552 (7683), 88–91.

Cherchneff, I., Barker, J.R., Tielens, A.G., 1992. Polycyclic aromatic hydrocarbon formation in carbon-rich stellar envelopes. Astrophys. J. 401, 269–287.

Claire, M.W., Sheets, J., Cohen, M., Ribas, I., Meadows, V.S., Catling, D.C., 2012. The evolution of solar flux from 0.1 nm to 160 μm: quantitative estimates for planetary studies. Astrophys. J. 757 (1), 95.

Cnossen, I., Sanz-Forcada, J., Favata, F., Witasse, O., Zegers, T., Arnold, N.F., 2007. Habitat of early life: Solar X-ray and UV radiation at Earth's surface 4–3.5 billion years ago. J. Geophys. Res.: Planets 112 (E2).

Cockell, C.S., 2000. The ultraviolet history of the terrestrial planets?implications for biological evolution. Planet. Space Sci. 48 (2–3), 203–214.

Cottin, H., Moore, M.H., Bénilan, Y., 2003. Photodestruction of relevant interstellar molecules in ice mixtures. Astrophys. J. 590 (2), 874.

Cruz-Diaz, G.A., Ricca, A., Mattioda, A.L., 2020. Polycyclic aromatic hydrocarbons and dust particle surface interactions: Catalytic hydrogenation of polycyclic aromatic hydrocarbon molecules under vacuum conditions. ACS Earth Space Chem. 4 (10), 1730–1742.

Davies, G.F., 1992. On the emergence of plate tectonics. Geology 20 (11), 963–966.

Dong, D., Li, P., Li, X., Xu, C., Gong, D., Zhang, Y., Zhao, Q., Li, P., 2010a. Photocatalytic degradation of phenanthrene and pyrene on soil surfaces in the presence of nanometer rutile TiO2 under UV-irradiation. Chem. Eng. J. 158 (3), 378–383.

Dong, D., Li, P., Li, X., Zhao, Q., Zhang, Y., Jia, C., Li, P., 2010b. Investigation on the photocatalytic degradation of pyrene on soil surfaces using nanometer anatase TiO2 under UV irradiation. J. Hard Mater. 174 (1–3), 859–863.

dos Santos, R., Patel, M., Cuadros, J., Martins, Z., 2016. Influence of mineralogy on the preservation of amino acids under simulated Mars conditions. Icarus 277, 342–353.

Ehrenfreund, P., Rasmussen, S., Cleaves, J., Chen, L., 2006. Experimentally tracing the key steps in the origin of life: The aromatic world. Astrobiology 6 (3), 490–520.

Eigenbrode, J.L., Summons, R.E., Steele, A., Freissinet, C., Millan, M., Navarro-González, R., Sutter, B., McAdam, A.C., Franz, H.B., Glavin, D.P., et al., 2018. Organic matter preserved in 3-billion-year-old mudstones at Gale crater, Mars. Science 360 (6393), 1096–1101.

Fenton, H.J.H., 1894. LXXIII.-Oxidation of tartaric acid in presence of iron. J. Chem. Soc. Trans. 65, 899–910.

Flynn, G., 1996. Sources of 10 micron interplanetary dust: The contribution from the Kuiper belt. In: International Astronomical Union Colloquium, Vol. 150. Cambridge University Press, pp. 171–175.

Flynn, G., Keller, L., Jacobsen, C., Wirick, S., 2004. An assessment of the amount and types of organic matter contributed to the Earth by interplanetary dust. Adv. Space Res. 33 (1), 57–66.
Fornaro, T., Boosman, A., Brucato, J.R., ten Kate, I.L., Siljeström, S., Poggiali, G., Steele, A., Hazen, R.M., 2018a. UV irradiation of biomarkers adsorbed on minerals under Martian-like conditions: Hints for life detection on Mars. Icarus 313, 38–60.
Fornaro, T., Brucato, J.R., Poggiali, G., Corazzi, M.A., Biczysko, M., Jaber, M., Foustoukos, D.I., Hazen, R.M., Steele, A., 2020. UV irradiation and near infrared characterization of laboratory Mars soil analog samples. Front. Astron. Space Sci. 7, 539289.
Fornaro, T., Steele, A., Brucato, J.R., 2018b. Catalytic/protective properties of martian minerals and implications for possible origin of life on Mars. Life 8 (4), 56.
Frantseva, K., Mueller, M., ten Kate, I.L., van der Tak, F.F., Greenstreet, S., 2018. Delivery of organics to Mars through asteroid and comet impacts. Icarus 309, 125–133.
Freissinet, C., Glavin, D., Mahaffy, P.R., Miller, K., Eigenbrode, J., Summons, R., Brunner, A., Buch, A., Szopa, C., Archer, Jr., P., et al., 2015. Organic molecules in the sheepbed mudstone, gale crater, mars. J. Geophys. Res.: Planets 120 (3), 495–514.
Frenklach, M., Feigelson, E.D., 1989. Formation of polycyclic aromatic hydrocarbons in circumstellar envelopes. Astrophys. J. 341, 372–384.
Frost, R.L., Kloprogge, J.T., Ding, Z., 2002. The Garfield and Uley nontronites?An infrared spectroscopic comparison. Spectrochim. Acta A 58 (9), 1881–1894.
Fujishima, A., Rao, T.N., Tryk, D.A., 2000. Titanium dioxide photocatalysis. J. Photochem. Photobiol. C: Photochem. Rev. 1 (1), 1–21.
Gauger, T., Konhauser, K., Kappler, A., 2015. Protection of phototrophic iron (II)-oxidizing bacteria from UV irradiation by biogenic iron (III) minerals: Implications for early Archean banded iron formation. Geology 43 (12), 1067–1070.
Geatches, D., Clark, S., Greenwell, H., 2012. Iron reduction in nontronite-type clay minerals: Modelling a complex system. Geochim. Cosmochim. Acta 81, 13–27.
Giese, C.-C., Ten Kate, I.L., Plümper, O., King, H.E., Lenting, C., Liu, Y., Tielens, A.G., 2019. The evolution of polycyclic aromatic hydrocarbons under simulated inner asteroid conditions. Meteorit. Planet. Sci. 54 (9), 1930–1950.
Glavin, D.P., Alexander, C.M., Aponte, J.C., Dworkin, J.P., Elsila, J.E., Yabuta, H., 2018. The origin and evolution of organic matter in carbonaceous chondrites and links to their parent bodies. In: Primitive Meteorites and Asteroids. Elsevier, pp. 205–271.
Grotzinger, J.P., Sumner, D.Y., Kah, L., Stack, K., Gupta, S., Edgar, L., Rubin, D., Lewis, K., Schieber, J., Mangold, N., et al., 2014. A habitable fluvio-lacustrine environment at Yellowknife Bay, Gale Crater, Mars. Science 343 (6169).
Hartman, H., 1975. Speculations on the origin and evolution of metabolism. J. Mol. Evol. 4 (4), 359–370.
Herzog, 2022. HP-MA: Automatic pulverizing mill. https://www.herzog-maschinenfabrik.de/en/products/hp-ma-automatic-pulverizing-mill/. Accessed: 2019-09-30.
Huang, W., Ferris, J.P., 2006. One-step, regioselective synthesis of up to 50-mers of RNA oligomers by montmorillonite catalysis. J. Am. Chem. Soc. 128 (27), 8914–8919.
Hudgins, D.M., Allamandola, L., 1997. Infrared spectroscopy of matrix-isolated polycyclic aromatic hydrocarbon cations. 4. The tetracyclic PAH isomers chrysene and 1, 2-benzanthracene. J. Phys. Chem. A 101 (19), 3472–3477.
Hudgins, D.M., Sandford, S.A., 1998. Infrared spectroscopy of matrix isolated polycyclic aromatic hydrocarbons. 1. PAHs containing two to four rings. J. Phys. Chem. A 102 (2), 329–343.
Jenniskens, P., Wilson, M.A., Packan, D., Laux, C.O., Krüger, C.H., Boyd, I.D., Popova, O.P., Fonda, M., 2000. Meteors: A delivery mechanism of organic matter to the early Earth. In: Leonid Storm Research. Springer, pp. 57–70.
Jia, H., Zhao, J., Fan, X., Dilimulati, K., Wang, C., 2012. Photodegradation of phenanthrene on cation-modified clays under visible light. Appl. Catal. B 123, 43–51.
Jia, H., Zhao, S., Shi, Y., Zhu, K., Gao, P., Zhu, L., 2019. Mechanisms for light-driven evolution of environmentally persistent free radicals and photolytic degradation of PAHs on Fe (III)-montmorillonite surface. J. Hard Mater. 362, 92–98.
Jia, H., Zhao, S., Shi, Y., Zhu, L., Wang, C., Sharma, V.K., 2018. Transformation of polycyclic aromatic hydrocarbons and formation of environmentally persistent free radicals on modified montmorillonite: the role of surface metal ions and polycyclic aromatic hydrocarbon molecular properties. Environ. Sci. Technol. 52 (10), 5725–5733.
Juntunen, H.L., Leinen, L.J., Pitts, B.K., O?Hanlon, S.M., Theiling, B.P., Barge, L.M., Videau, P., Gaylor, M.O., 2018. Investigating the kinetics of Montmorillonite clay-catalyzed conversion of anthracene to 9, 10-anthraquinone in the context of prebiotic chemistry. Orig. Life Evol. Biospheres 48 (3), 321–330.
Keeling, J.L., Raven, M.D., Gates, W.P., 2000. Geology and characterization of two hydrothermal nontronites from weathered metamorphic rocks at the Uley graphite mine, South Australia. Clays Clay Miner. 48 (5), 537–548.
Kloprogge, J.T.T., Hartman, H., 2022. Clays and the origin of life: The experiments. Life 12 (2), 259.
Kofman, V., Witlox, M., Bouwman, J., Ten Kate, I., Linnartz, H., 2018. A multifunctional setup to record FTIR and UV-vis spectra of organic molecules and their photoproducts in astronomical ices. Rev. Sci. Instrum. 89 (5), 053111.
Kumar, B.S., Dhakshinamoorthy, A., Pitchumani, K., 2014. K10 montmorillonite clays as environmentally benign catalysts for organic reactions. Catal. Sci. Technol. 4 (8), 2378–2396.
Laszlo, P., 1987. Chemical reactions on clays. Science 235 (4795), 1473–1477.
Lear, P.R., Stucki, J.W., 1989. Effects of iron oxidation state on the specific surface area of nontronite. Clays Clay Miner. 37 (6), 547–552.
Lecasble, M., Remusat, L., Viennet, J.-C., Laurent, B., Bernard, S., 2022. Polycyclic aromatic hydrocarbons in carbonaceous chondrites can be used as tracers of both pre-accretion and secondary processes. Geochim. Cosmochim. Acta 335, 243–255.
Linsebigler, A.L., Lu, G., Yates Jr., J.T., 1995. Photocatalysis on TiO2 surfaces: principles, mechanisms, and selected results. Chem. Rev. 95 (3), 735–758.
Liu, R., Xiao, D., Guo, Y., Wang, Z., Liu, J., 2014. A novel photosensitized Fenton reaction catalyzed by sandwiched iron in synthetic nontronite. RSC Adv. 4 (25), 12958–12963.
Madejová, J., 2003. FTIR techniques in clay mineral studies. Vib. Spectrosc. 31 (1), 1–10.
Marty, B., Alexander, C.M.O., Raymond, S.N., 2013. Primordial origins of Earth?s carbon. Rev. Mineral. Geochem. 75 (1), 149–181.
Mattioda, A.L., Cruz-Diaz, G.A., Ging, A., Barnhardt, M., Boersma, C., Allamandola, L.J., Schneider, T., Vaughn, J., Phillips, B., Ricca, A., 2020b. Formation of Complex Organic Molecules (COMs) from Polycyclic Aromatic Hydrocarbons (PAHs): Implications for ISM IR emission plateaus and solar system organics. ACS Earth Space Chem. 4 (12), 2227–2245.
Mattioda, A., Hudgins, D., Boersma, C., Bauschlicher, C., Ricca, A., Cami, J., Peeters, E., de Armas, F.S., Saborido, G.P., Allamandola, L., 2020a. The NASA ames PAH IR spectroscopic database: the laboratory spectra. Astrophys. J. Suppl. Ser. 251 (2), 22.
Moldoveanu, S.C., 2009. Pyrolysis of Organic Molecules: Applications to Health and Environmental Issues. Elsevier.
Murchie, S.L., Seelos, F.P., Hash, C.D., Humm, D.C., Malaret, E., McGovern, J.A., Choo, T.H., Seelos, K.D., Buczkowski, D.L., Morgan, M.F., et al., 2009. Compact Reconnaissance Imaging Spectrometer for Mars investigation and data set from the Mars Reconnaissance Orbiter's primary science phase. J. Geophys. Res.: Planets 114 (E2).
Nagendrappa, G., et al., 2002. Organic synthesis using clay catalysts: clays for ?Green Chemistry? Resonance-J. Sci. Educ. 7 (1).
Ohno, T., Tokieda, K., Higashida, S., Matsumura, M., 2003. Synergism between rutile and anatase TiO2 particles in photocatalytic oxidation of naphthalene. Appl. Catal. A 244 (2), 383–391.
Okumura, F., Mimura, K., 2011. Gradual and stepwise pyrolyses of insoluble organic matter from the Murchison meteorite revealing chemical structure and isotopic distribution. Geochim. Cosmochim. Acta 75 (22), 7063–7080.
O'Neil, J., Carlson, R.W., Francis, D., Stevenson, R.K., 2008. Neodymium-142 evidence for Hadean mafic crust. Science 321 (5897), 1828–1831.
Pearson, V.K., Sephton, M.A., Kearsley, A.T., Bland, P.A., Franchi, I.A., Gilmour, I., 2002. Clay mineral-organic matter relationships in the early solar system. Meteorit. Planet. Sci. 37 (12), 1829–1833.
Pendleton, Y.J., Allamandola, L.J., 2002. The organic refractory material in the diffuse interstellar medium: Mid-infrared spectroscopic constraints. Astrophys. J. Suppl. Ser. 138 (1), 75.
Pierson, B.K., Mitchell, H.K., Ruff-Roberts, A.L., 1993. Chloroflexus aurantiacus and ultraviolet radiation: implications for archean shallow-water stromatolites. Orig. Life Evol. Biosphere 23 (4), 243–260.
Poch, O., Jaber, M., Stalport, F., Nowak, S., Georgelin, T., Lambert, J.-F., Szopa, C., Coll, P., 2015. Effect of nontronite smectite clay on the chemical evolution of several organic molecules under simulated martian surface ultraviolet radiation conditions. Astrobiology 15 (3), 221–237.
Poggiali, G., Fornaro, T., Potenti, S., Corazzi, M.A., Brucato, J.R., 2020. Ultraviolet photoprocessing of glycine adsorbed on various space-relevant minerals. Front. Astron. Space Sci. 7, 18.
Potenti, S., Manini, P., Fornaro, T., Poggiali, G., Crescenzi, O., Napolitano, A., Brucato, J.R., Barone, V., d?Ischia, M., 2018. Solid state photochemistry of hydroxylated naphthalenes on minerals: probing polycyclic aromatic hydrocarbon transformation pathways under astrochemically-relevant conditions. ACS Earth Space Chem. 2 (10), 977–1000.
Poulet, F., Carter, J., Bishop, J., Loizeau, D., Murchie, S., 2014. Mineral abundances at the final four curiosity study sites and implications for their formation. Icarus 231, 65–76.
Razzell Hollis, J., Fornaro, T., Rapin, W., Wade, J., Vicente-Retortillo, Á., Steele, A., Bhartia, R., Beegle, L.W., 2021. Detection and degradation of adenosine monophosphate in perchlorate-spiked martian regolith analog, by deep-ultraviolet spectroscopy. Astrobiology 21 (5), 511–525.
Remusat, L., Derenne, S., Robert, F., Knicker, H., 2005. New pyrolytic and spectroscopic data on Orgueil and Murchison insoluble organic matter: A different origin than soluble? Geochim. Cosmochim. Acta 69 (15), 3919–3932.
Ruppert, G., Bauer, R., Heisler, G., 1993. The photo-Fenton reaction — an effective photochemical wastewater treatment process. J. Photochem. Photobiol. A: Chem. 73 (1), 75–78.
Scappini, F., Casadei, F., Zamboni, R., Franchi, M., Gallori, E., Monti, S., 2004. Protective effect of clay minerals on adsorbed nucleic acid against UV radiation: possible role in the origin of life. Int. J. Astrobiol. 3 (1), 17–19.
SDBS, 2022. SDBSWeb. https://sdbs.db.aist.go.jp. Accessed: 2020-09-30.

Sephton, M.A., 2002. Organic compounds in carbonaceous meteorites. Nat. Prod. Rep. 19 (3), 292–311.
Shkrob, I.A., Chemerisov, S.D., 2009. Light induced fragmentation of polyfunctional carboxylated compounds on hydrated metal oxide particles: from simple organic acids to peptides. J. Phys. Chem. C 113 (39), 17138–17150.
Shkrob, I.A., Marin, T.M., Adhikary, A., Sevilla, M.D., 2011a. Photooxidation of nucleic acids on metal oxides: Physicochemical and Astrobiological Perspectives. J. Phys. Chem. C 115 (8), 3393–3403.
Shkrob, I.A., Marin, T.W., Chemerisov, S.D., Sevilla, M.D., 2011b. Mechanistic aspects of photooxidation of polyhydroxylated molecules on metal oxides. J. Phys. Chem. C 115 (11), 4642–4648.
Sỳkora, J., 1997. Photochemistry of copper complexes and their environmental aspects. Coord. Chem. Rev. 159, 95–108.
Szczepanski, J., Chapo, C., Vala, M., 1993. Visible and infrared spectra of matrix-isolated perylene cations. Chem. Phys. Lett. 205 (4–5), 434–439.
ten Kate, I.L., Garry, J.R., Peeters, Z., Quinn, R., Foing, B., Ehrenfreund, P., 2005. Amino acid photostability on the Martian surface. Meteorit. Planet. Sci. 40 (8), 1185–1193.
Theng, B.K., 2018. Clay Mineral Catalysis of Organic Reactions. CRC Press.
Thomson, B., Bridges, N., Milliken, R., Baldridge, A., Hook, S., Crowley, J., Marion, G., de Souza Filho, C., Brown, A., Weitz, C., 2011. Constraints on the origin and evolution of the layered mound in Gale Crater, Mars using Mars Reconnaissance Orbiter data. Icarus 214 (2), 413–432.
Tielens, A.G., 2008. Interstellar polycyclic aromatic hydrocarbon molecules. Annu. Rev. Astron. Astrophys. 46, 289–337.
Tielens, A., 2013. The molecular universe. Rev. Modern Phys. 85 (3), 1021.
Tu, V.M., Rampe, E.B., Bristow, T.F., Thorpe, M.T., Clark, J.V., Castle, N., Fraeman, A.A., Edgar, L.A., McAdam, A., Bedford, C., et al., 2021. A review of the phyllosilicates in Gale Crater as detected by the CheMin instrument on the Mars Science Laboratory, Curiosity rover. Minerals 11 (8), 847.
Vicente-Retortillo, A., Martínez, G., Rennó, N.O., Lemmon, M., de la Torre-Juárez, M., Gómez-Elvira, J., 2020. In situ UV measurements by MSL/REMS: dust deposition and angular response corrections. Space Sci. Rev. 216 (5), 1–19.
Vicente-Retortillo, Á., Valero, F., Vázquez, L., Martínez, G.M., 2015. A model to calculate solar radiation fluxes on the Martian surface. J. Space Weather Space Clim. 5, A33.
Wang, Y., Liu, C., Li, F., Liu, C., Liang, J., 2009. Photodegradation of polycyclic aromatic hydrocarbon pyrene by iron oxide in solid phase. J. Hard Mater. 162 (2–3), 716–723.
Wen, S., Zhao, J., Sheng, G., Fu, J., et al., 2002. Photocatalytic reactions of phenanthrene at TiO2/water interfaces. Chemosphere 46 (6), 871–877.
Whittet, D., 1997. Is extraterrestrial organic matter relevant to the origin of life on Earth? In: Planetary and Interstellar Processes Relevant to the Origins of Life. Springer, pp. 249–262.
Yap, C.L., Gan, S., Ng, H.K., 2011. Fenton based remediation of polycyclic aromatic hydrocarbons-contaminated soils. Chemosphere 83 (11), 1414–1430.
Zhang, L., Li, P., Gong, Z., Li, X., 2008. Photocatalytic degradation of polycyclic aromatic hydrocarbons on soil surfaces using TiO2 under UV light. J. Hard Mater. 158 (2–3), 478–484.
Zhang, L., Xu, C., Chen, Z., Li, X., Li, P., 2010. Photodegradation of pyrene on soil surfaces under UV light irradiation. J. Hard Mater. 173 (1–3), 168–172.